Deliverable Number:	D8.7
Deliverable Title:	Compact Instrumentation for Larmor Labelling applications at the ESS.
Delivery date:	Month 31 (5/18/2018)
Leading beneficiary:	TUD
Dissemination level:	Public
Status:	version **FINAL**
Authors:	André Kusmin, Jeroen Plomp, Michel Thijs, Catherine Pappas (TUD)

Project number:	654000
Project acronym:	SINE2020
Project title:	Worldclass Science and Innovation with Neutrons in Europe 2020
Starting date:	1st of October 2015
Duration:	48 months
Call identifier:	H2020-INFRADEV-2014-2015
Funding scheme:	Combination of CP & CSA – Integrating Activities

This project has received funding from the European Union's Horizon 2020 research and innovation programme under grant agreement No 654000

1. Introduction

Larmor labelling is widely used to increase the resolution of neutron scattering both in energy (Neutron Spin Echo spectroscopy [1]) and momentum transfer (Spin Echo SANS [2], Larmor diffraction [3]). Since these techniques do not require highly monochromatized and collimated neutron beams they do not trade resolution for neutron flux. However, the effective neutron count rate is effectively reduced because of the use of polarised neutron beams and because the Larmor precession areas cannot be combined with neutron guides. Furthermore, most existing instruments are relatively long, due to homogeneity requirements for the precession areas. This in fact collimates the beam and significantly reduces the neutron flux.

Larmor labelling uses the precession phase of the neutron beam polarization $\vec{P}$ around the magnetic field $\vec{B}$ to directly measure the energy or the momentum transfer at the sample. For this purpose $\vec{P}$ should be non-collinear to $\vec{B}$, in the optimal case the two vectors should be orthogonal to each other. In this case and for the weak magnetic fields commonly used in neutron scattering, $\vec{P}$ would precess around $\vec{B}$ following the classical equation of motion:

$$d\vec{P}/dt = \gamma\, \vec{P} \times \vec{B} = \vec{P} \times \vec{\omega}_L, \quad [1]$$

where γ = -183.2 rad MHz T^{-1} is the neutron gyromagnetic ratio. We note that this description is also quantum mechanically correct because $\vec{P}$ is an observable and as such it follows the equations of motion of classical mechanics according to the Ehrenfest theorem.

If the neutron beam has a velocity $\mathrm{v} = h/m\lambda = \sqrt{2\epsilon}/m$, with λ the corresponding wavelength, ϵ the energy, m the neutron mass and h the Planck constant, it will cover a distance $\ell = \mathrm{v}\,\mathrm{t}$ over a time lapse t. If over this distance a homogeneous magnetic field is applied, the accumulated Larmor phase is given by:

$$\varphi = \omega_L t = \gamma B\, \ell/\mathrm{v} = (\gamma m/h)\, \lambda\, B\, \ell = \gamma\, B\, \ell\, m/\sqrt{2\epsilon}. \quad [2]$$

Thus φ encodes both the energy and the trajectory of the beam through the magnetic field region. If the magnetic field is not homogeneous but its direction changes along the neutron trajectory, e.g. by an angle a_g, one may associate to this change a geometric rotation frequency, $\omega_g = da_g/dt = \mathrm{v}\; da_g/d\,\ell$, which thus depends on the velocity of the neutron beam [4]. The ratio between ω_L and ω_g defines the adiabaticity parameter: $k = \omega_L/\omega_g$, which as a rule of thumb should be $k \gtrsim 10$ and $k \lesssim 0.1$ for the adiabatic and non-adiabatic limits respectively. The intermediate case, where both frequencies are comparable should be avoided, as its outcome cannot be easily estimated.

Most instruments measure the difference in precession angles accumulated before and after scattering, $\Delta\varphi = \varphi_1 - \varphi_2$. They also adopt magnetic field designs that disentangle the energy transfer contribution to $\Delta\varphi$ from the one arising from the momentum transfer. NSE spectrometers ideally encode only energy transfer and SESANS or Larmor diffraction setups the change of trajectories due to the scattering process. Despite these differences, a common challenge for all designs is to reach the highest possible resolution by creating highly homogeneous magnetic fields over large beam cross sections. Magnetic field inhomogeneities and design imperfections introduce a spread in precession angles and ultimately reduce the normalised modulation after precession in the spectrometer:

$$P_{NSE} = P\, \cos\,(\Delta\varphi) \quad [3]$$

where $P_{NSE} = 1$ for an ideally polarised neutron beam ($P = 1$) and ideally homogeneous magnetic fields.

From Eq. 2 it appears that the important parameter for Larmor labelling instrumentation is the magnetic field integral $B\,\ell$, for a varying magnetic field $\int B(\ell)\, d\ell$, which should be ideally the same for all neutron trajectories. In the following we use magnetic field calculations to evaluate the performance of two compact magnetic field configurations, one for NSE spectroscopy and another

one for SESANS. Both configurations would combine high performance and high brilliance and would lead to new instrument designs for monochromatic and wide-band (time-of-flight) operation. These designs would be of particular relevance to the ESS, where the flat pancake moderators results in high intensity neutron beams confined in a small cross-section, well-adapted to small samples and compact instrumentation.

2. A Compact Neutron Spin Echo Spectrometer

In NSE spectrometers the precession magnetic fields are longitudinal, produced by solenoids, with low intrinsic magnetic field integral inhomogeneities. Nevertheless, the homogeneity requirements for long Fourier times cannot be reached without the help of Fresnel coils [5]. The challenge consists in realising high field integrals with the highest possible homogeneity, thus with the smallest possible trajectory-dependence of $\Delta\varphi$. In the following we will discuss the influence of some magnetic coil design parameters on P_{NSE} with focus on the repercussions of compact neutron beams.

The magnetic field integral inhomogeneities arise from (a) the intrinsic inhomogeneity of the magnetic field, which leads to different precession angles for parallel neutron trajectories of the same length and (b) the beam size and divergence, which leads to a spread in trajectory lengths and thus to different precession angles even in an ideally homogeneous magnetic field. The separation of these two effects was considered by Zeyen [6] and, recently and in more details, by Pasini et al.[7] In this work we considered these two effects in a more general fashion and assessed:

1. the feasibility of a compact design of a NSE spectrometer, and
2. implications of using a pancake moderator which is currently planned for ESS.

The magnetic field configuration considered is schematically shown in Fig. 1. This is the first arm of an NSE spectrometer, where the neutron beam exits a polarizing neutron guide, leading to $P = 1$. The precessions start at the $\pi/2$ flipper, which is positioned at a distance a_1 from the blue rectangular shape representing the main coil of length L and radius R. A π flipper between the main coil and the sample, at a distance a_2 from the end of the coil, marks the reversal point of the precessions. Additional coils, modeled by current loops, lower the magnetic field at the positions of the π/2 and π-flippers. In the calculations the efficiency of the flippers was assumed to be 100% and thus their intrinsic adiabaticity was ignored. Besides the flippers all magnetic fields are longitudinal and the magnetic field configuration is adiabatic. The symmetry of the setup with respect to $x = 0$, i.e. the center of the coil, is quantified by the parameter $s = (d_1 + L/2)/(d_1 + L + d_2)$, which is $s = 1/2$ for he symmetric case $d_1 = d_2$.

This configuration can be optimised as such and is also representative for the symmetric setup placed after the sample. Indeed, in NSE spectroscopy there is not correlation between the neutron beam trajectories before and after the sample, thus the magnetic configuration of each arm of the spectrometer must be optimised indepently from the other arm.

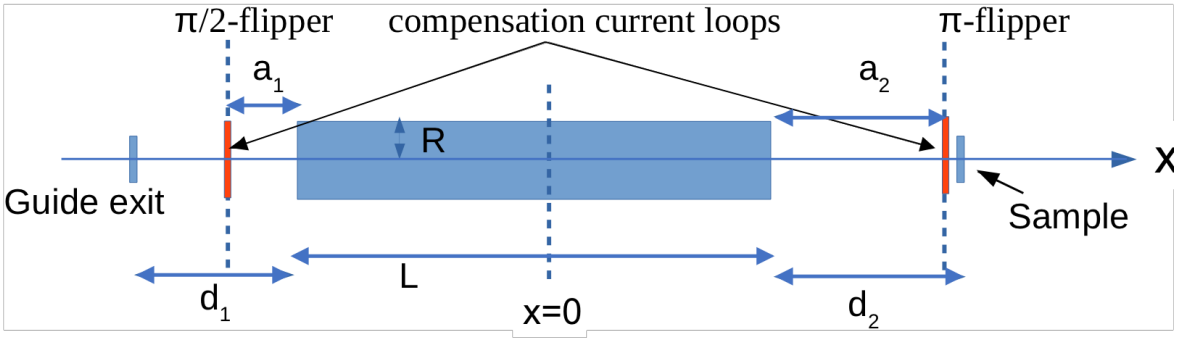

Fig. 1: Schematic representation of the configuration considered for the first arm of a NSE spectrometer. The layout is characterized by the lengths L, a_1, a_2 and R. The blue rectangular area represents the main precession coil.

The semi-analytical calculations were performed using RADIA [8] and Mathematica. The starting point was the total magnetic field integral between the $\pi/2$ and the π flipper at the symmetry axis of the setup $J_0 = \int B_{(x,0,0)}(x)\, dx$. The magnetic field inhomogeneities have been calculated for :

(a) the parallel trajectories $H = \int \beta(x)\, dx$,
(b) the divergence of the beam $G = J_0/2 + \int [x^2 \beta(x)]\, dx$, and
(c) the crossed term $U = \int x\, \beta(x)\, dx$

with $\beta(x) = \frac{1}{8}\frac{1}{B_x(x)}\left(\frac{\partial B_x(x)}{\partial x}\right)^2 - \frac{1}{4}\frac{\partial^2 B_x(x)}{\partial^2 x}$.

If a specific neutron trajectory enters the precession area at a distance y_0 and $z_0$from the x-axis and with an angle θ to the x-axis and, the difference in the magnetic field integral that can be written as:

$$\Delta J = J - J_0 = H\, r_0^2 + G\, \tan^2\theta + 2\, U \left[y_0 \tan\theta_y + z_0 \tan\theta_z\right], \quad [4]$$

with $r_0^2 = y_0^2 + z_0^2$. One can thus calculate the variance of the magnetic field integral over the beam

$$\begin{aligned}\langle \Delta J^2 \rangle = {} & H^2 \langle r_0^4 \rangle + G^2 \langle \tan^4\theta \rangle + 4HG\, \langle r_0^2 \tan^2\theta \rangle + 4HU\, \langle r_0^2 \left[y_0 \tan\theta_y + z_0 \tan\theta_z\right] \rangle \\ & + 4GU\, \langle \tan^2\theta \left(y_0 \tan\theta_y + z_0 \tan\theta_z\right) \rangle + \\ & 4U^2 \left[\langle \left(y_0 \tan\theta_y\right)^2 \rangle + \langle (z_0 \tan\theta_z)^2 \rangle + 2 \langle y_0 z_0 \tan\theta_y \tan\theta_z \rangle \right] \end{aligned} \quad [5]$$

The goal is to minimise $\langle \Delta J^2 \rangle$ for the specific beam characteristics defined by the cross-sections of the guide (of width A_G and height B_G, or of radius R_G), the sample (of width A_S and height B_S, or of radius R_s), and the distances between them.

a. Symmetric magnetic layout

We fist consider the symmetric configuration, where $a_1 = a_2$ and $U = 0$. The influence of the beam geometry on the relevant parameters of Eq. 5 is given in Table I. It thus appears that, irrespective of the relative importance of the terms that contribute to eq. 5, a decrease in $\langle \Delta J^2 \rangle$ by a factor of ~ 3 can be achieved by using a rectangular beam cross-section with a height to width ratio of 1:4 instead of a square one. In the latter case (lower part of Table I), the inhomogeneities are reduced by at least a factor of ~ 3 with respect to the case where the beam height to width ratio is 1.

TABLE I. General expressions for beam averages calculated for rectangular (width A_G, A_S and height B_G, B_S) and circular cross-sections (radii R_G, R_S) of the guide and sample respectively. The results are given for a sample size equal and much smaller than that of the guide exit. The results correspond to the symmetric beam setup with s = 1/2.

averages & conditions	guide shape				
	rectangle	pancake ($B_G \to 0$)	$B_G = A_G/4$	square ($B_G = A_G$)	circle
sample size is the same as of the guide exit	$A_S = A_G, B_S = B_G$				$R_S = R_G$
$\langle r_0^4 \rangle$	$\frac{6A_G^4+5A_G^2B_G^2+6B_G^4}{90}$	$0.067\ A_G^4$	$0.070\ A_G^4$	$0.189\ A_G^4$	$0.1042\ R_G^4$
$\langle r_0^2 \tan^2\theta \rangle L_{tot}^2$	$\frac{2A_G^4+10A_G^2B_G^2+2B_G^4}{45}$	$0.044\ A_G^4$	$0.058\ A_G^4$	$0.311\ A_G^4$	$0.1667\ R_G^4$
$\langle \tan^4\theta \rangle L_{tot}^4$	$\frac{8(6A_G^4+5A_G^2B_G^2+6B_G^4)}{45}$	$1.07 A_G^4$	$1.13\ A_G^4$	$3.02\ A_G^4$	$1.67\ R_G^4$
sample is much smaller than the guide exit	$A_S \to 0, B_S \to 0$				$R_S \to 0$
$\langle r_0^4 \rangle$	$\frac{9A_G^4+10A_G^2B_G^2+9B_G^4}{720}$	$0.0125\ A_G^4$	$0.0134\ A_G^4$	$0.0389\ A_G^4$	$0.0208\ R_G^4$
$\langle r_0^2 \tan^2\theta \rangle L_{tot}^2$	$\frac{9A_G^4+10A_G^2B_G^2+9B_G^4}{180}$	$0.05\ A_G^4$	$0.054\ A_G^4$	$0.156\ A_G^4$	$0.0833\ R_G^4$
$\langle \tan^4\theta \rangle L_{tot}^4$	$\frac{9A_G^4+10A_G^2B_G^2+9B_G^4}{45}$	$0.2\ A_G^4$	$0.215\ A_G^4$	$0.622\ A_G^4$	$0.3333\ R_G^4$

b. Asymmetric magnetic layout

In general, the magnetic layout is asymmetric. In this general case, where $s \neq 1/2$, the optimum s-values change with the relative dimensions of the sample and the guide exits. Furthermore, these values are not the same for $\langle r_0^4 \rangle$ and $\langle r_0^2 \tan^2 \theta \rangle$ as it can be seen in Fig. 2. Thus, the optimum s-parameter is different for smaller or larger A_S/A_G ratios.

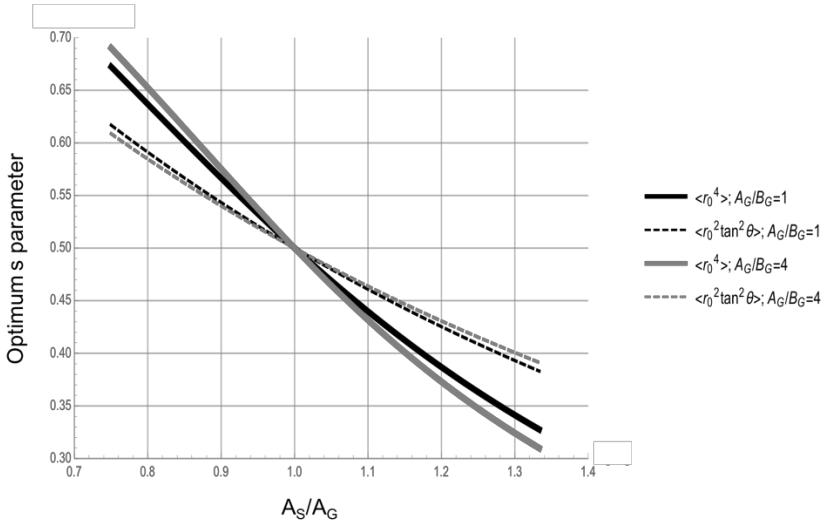

Fig. 2: Dependence of the optimum s, obtained by optimising the averages $\langle r_0^4 \rangle$ and $\langle r_0^2 \, tan^2 \, \theta \rangle$, on the ratio of sample over guide exit widths A_S/A_G The aspect ratio of the guide exit is A_G/B_G, and the ratio of the sample and guide exit sizes is $A_S/A_G = B_S/B_G$.

c. Minimization of intrinsic magnetic field inhomogeneities

In order to optimize $\langle \Delta J^2 \rangle$ one must take into account the respective weights of the averages, $\langle r_0^4 \rangle$, $\langle \tan^4 \theta \rangle$ and $\langle r_0^2 \tan^2 \theta \rangle$, which depend on the magnetic layout, namely on H^2, G^2 and $2HG$. One can see that the dimensions of these parameters are different. In order to compare all pre-factors with the dimension [length^2] and thus evaluate their dependence on the dimensions of the setup we introduce $F_0 = H^2, F_1 = 4HU/L_{tot}$ $F_2 = 2HG/L_{tot}^2$, $F_3 = 4GU/L_{tot}^3$, $F_4 = G^2/L_{tot}^4$ and $F_{U2} = 4U^2/L_{tot}^2$, where $L_{tot} = d_1 + L + d_2$. In general, F_1, F_{U2} and F_3 are the most significant contributions to $\langle \Delta J^2 \rangle$. In the case of a weak asymmetry of $\mathrm{a}_1 = 0.3$ m and $\mathrm{a}_2 = 0.5$ m, the influence of the coil dimensions on these parameters and on F_0 is given in Fig. 3.

The results show that beam averages are always positive for F_{U2} and they may be either positive or negative, depending on the parameter s, and the relation between the guide exit and sample size, for F_1 and F_3. Thus, it is possible to find a combination of parameters for which the F_1 and F_3 terms lower $\langle \Delta J^2 \rangle$. However, it is not clear how this can be implemented and whether this effect will be significant.

The results of the beam averages show that there is a clear gain with the “pancake moderator” beams. In addition, circularly shaped sample and guide cross sections lead to lower field integral inhomogeneities in comparison to the square ones. This is not surprising, as all coils have circular shapes. However, in practice, guides have square or rectangular cross-sections and so do the detectors. In that case, it is possible to choose rectangular cross-sections with a height over width ratio, e.g. 1:4. This increases the homogeneity of the magnetic field integral by at least 30 % (estimation based on the leading contribution $F_0 \langle r_0^4 \rangle$), which is better that the result obtained for circular beam cross sections. Thus the choice of beam cross sections that mimic the “pancake moderator” beams seems to significantly improve the magnetic field integral homogeneities of a NSE spectrometer.

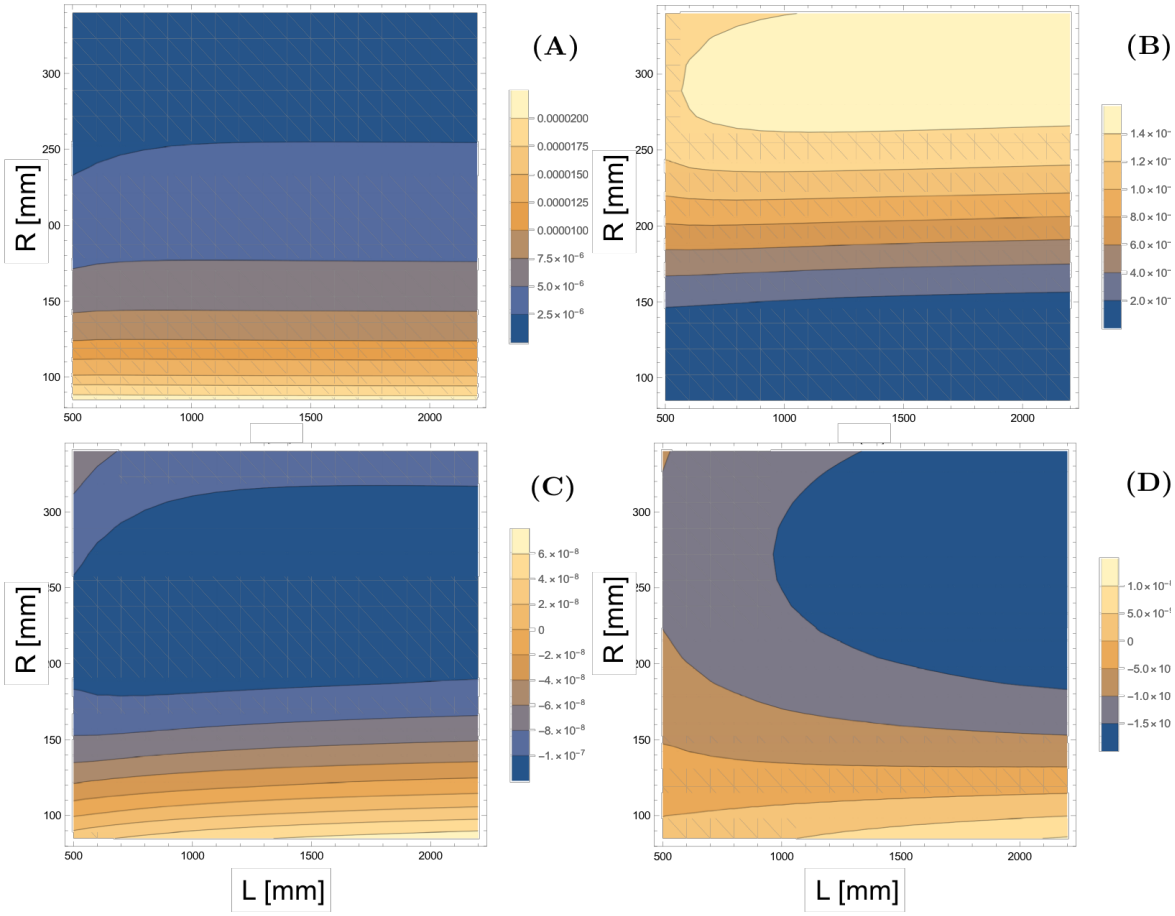

FIG. 3. Calculated contributions to the magnetic field inhomogeneity for an asymmetric magnetic layout of $a_1 = 0.3\ m$ *and* $a_2 = 0.5\ m$*. The contour plots indicate the dependence of the different parameters influencing the magnetic field inhomogeneities on the radius R and length L of the main precession coil. (A)* $F_0 = H^2$ *(B)* $F_{U2} = 4U^2/L_{tot}^2$*, (C)* $F_1 = 4HU/L_{tot}$ *and (D)* $F_3 = 4GU/L_{tot}^3$*.*

3. A Compact SEMSANS add-on for SANS and Imaging.

In this study we focused on the magnetic field arrangement of a compact Spin Echo Modulated Small Angle Neutron Scattering (SEMSANS) configuration [9, 10], that suits ideally to the neutron beams of the ESS flat pancake moderators. The advantage of SEMSANS is that it can be relatively compact and, can be installed as an add-on on a SANS or imaging instrument, upstream in front of the sample. Thus, it can be operated in parallel with the host SANS instrument allowing for the simultaneous coverage of a very broad range of length scales [11, 12].

Fig. 6 shows a schematic representation of the field arrangement considered in this study projected in the x-y plane (the coordinates are chosen such as that the neutron beam propagates along x direction and z is the vertical direction). It consists of two triangularly shaped magnetic field regions of similar shapes but of different sizes and magnetic fields. The first one, with magnetic field B_1, is larger whereas the second one, with magnetic field B_2, is shorter. It can be shown that the precession phases of all trajectories through the magnetic field arrangement depicted in Fig. 6 have constructive interference at the focus plane, when the following condition is fulfilled:

$$B_1 L_1 = B_2 L_2 , \tag{8}$$

Furthermore, the echo condition is fulfilled for all neutrons of all wavelengths that follow the central path illustrated by the horizontal dashed line in Fig. 6. The triangular shape of these field regions ensures the angular encoding of the neutron trajectories through the Larmor precession phase.

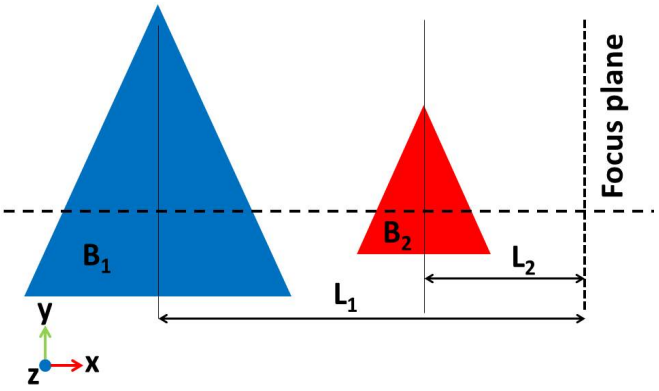

Figure 6: Schematic representation of the SEMSANS field configuration considered in this study. B_1 and B_2 are the respective magnetic fields of the first and second triangular field regions. The focus plane indicates the plane, where all cumulative precession phases interfere constructively. Ideally the focus plane should also be the detector plane. L1 and L2 are the distances of the focus plane from the magnetic centres of region 1 and 2 respectively. In the calculation, we have considered only those neutron trajectories that cross both triangular field regions

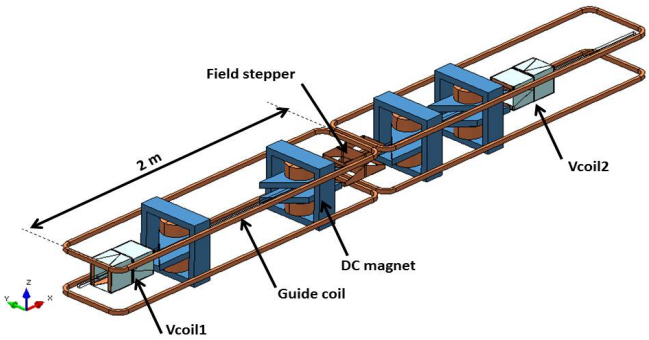

Figure 7: Schematic drawing of SEMSANS arrangement considered for the magnetic field calculations. The white boxes illustrate the Vcoils, which act as π/2 flippers, the blue components are DC magnets with parallelogram shaped pole shoes, the central coil is a field stepper. The long upper and lower create a homogenous magnetic field, which guides the beam polarisation.

Fig. 7 shows a 3D representation of such a setup. The configuration considered is based on two pairs of DC magnets with parallelogram pole shoes. Each pair simulates a triangular magnetic field region as shown in Fig. 6. The DC magnets include RF flippers, not shown in figure 7, that increase the sensitivity by zero field precession [13]: after the first RF flip and when leaving the first DC magnet, the neutron beam polarisation experiences an increase of magnetic field instead of an decrease. Consequently, in the region between the magnets the neutron beam polarisation experiences an effective precession field of strength $2B$ instead of the actually applied (relatively low) guide field. In the calculations the efficiency of the RF flippers was considered to be 100% (a reasonable value is 99.8% [14]) and their intrinsic adiabaticity was ignored. The adiabaticity calculations were therefore based only on the DC fields. As usual in SESANS setups, precessions start and end with π/2 flips performed using the so-called Vcoils [15], illustrated by the white boxes In Fig.7. A guide field has been applied along the whole setup using the large coils top and bottom, to ensure that the magnetic field is large and homogeneous enough to maintain the polarisation and precession phase of the neutron beam. A current screen field stepper [14,15] between the two pairs of DC magnets leads to a sudden reversal in the field direction with respect to the beam polarisation. This is the reversal point of the precessions and thus the magnetic symmetry point of the setup.

The magnetic field configuration of this setup has been calculated and optimised using the Infolytica MagNet software. All major components were included in the model, such as the guide field, Vcoils, DC magnets, field stepper. However the RF flippers were left out for the reasons mentioned above. The dimensions were chosen such as to correspond to a standard setup and may be easily scaled to investigate the effect of a compact beam size.

On the basis of the magnetic field calculations we first evaluated the adiabaticity parameter k over a representative neutron trajectory and for a wavelength of 0.2 nm, which would be the lowest wavelength limit for such a setup. The results are given in figure 8 and show that the adiabaticity condition ($k \gtrsim 10$) is fulfilled everywhere in the setup except at the position of the field stepper,

where $k \leq 0.1$ as indeed the transition should be non-adiabatic. Thus besides field stepper region on can safely assume the magnetic field configuration to be adiabatic and thus use Eq. 2.

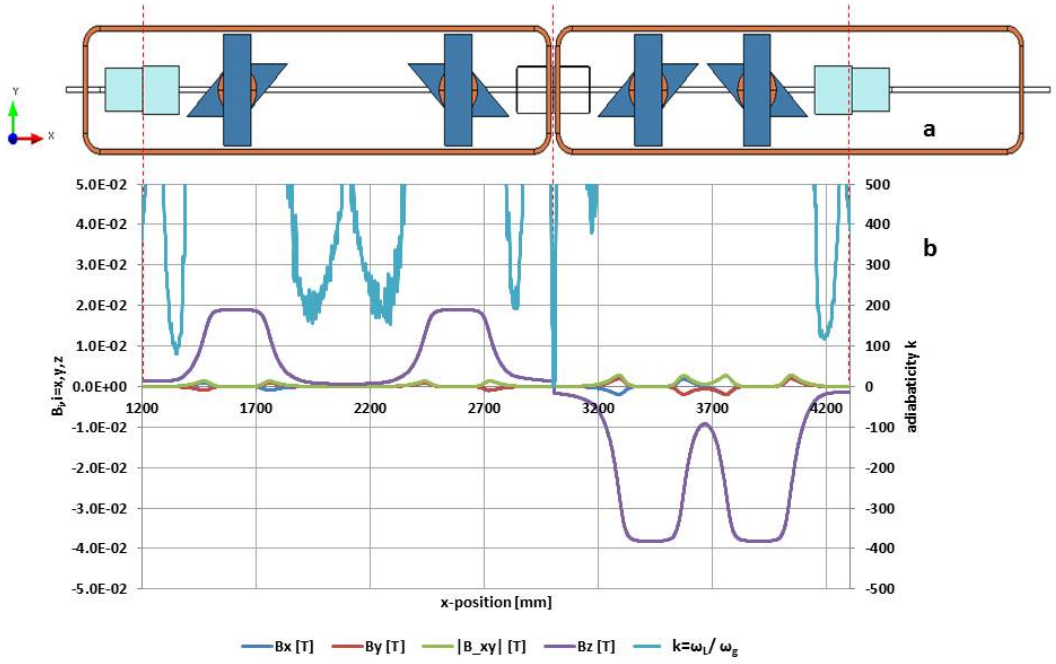

Figure 8: Top view of the SEMSANS setup (a) and (b) the corresponding magnetic field components $B_i, i = x, y, z$ *and adiabaticity parameter k for a path parallel to the symmetry x-axis and with an offset of y=5 mm and z=5 mm.*

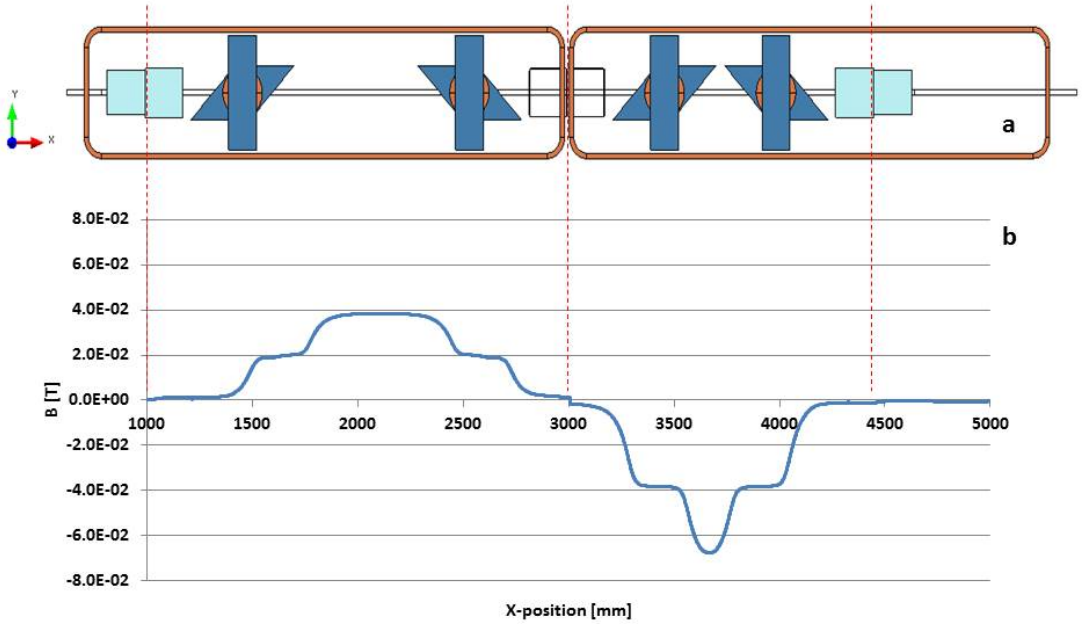

Figure 9: Top view of the arrangement (a) and (b) magnetic field modulus, B, along the central path of the neutron beam, i.e along x for z,y=0, as experienced by the neutron beam polarisation (i.e. after taking into account the zero field precession [13]).

When considering the magnetic field line-integral experienced by the neutron beam polarisation, the zero field precession induced by the RF flippers must be taken into account. This leads to the effective magnetic field shown in figure 8.

The calculation is optimised such that the integral of the central line (dotted line in Fig.6), i.e. the net surface under the plot of Fig. 9 is exactly zero. This means that the net phase for all wavelengths should be zero, which corresponds to the spin echo condition. For paths parallel to the central line the net phase varies as a function of the y-position and wavelength as illustrated by the contour plot of the NSE polarization amplitude given in Fig. 10. Thus, for exactly parallel paths there is no focussing condition as the phase is fixed by the specific y and x positions.

The effect of the beam divergence is illustrated on the example of 7 individual neutron trajectories shown in Fig. 11. The magnetic field integrals show the characteristic parabolic dependence of the magnetic field integral on the distance from the central line of the specific trajectories [5]. As for NSE spectroscopy, this magnetic field integral dependence on the specific neutron trajectories limits the performance of the setup as it reduces the NSE polarization Indeed, for each starting y-position the line-integral difference with respect to the central line will result in a wavelength dependent phase. The average of these phases for each individual wavelength will reduce the final P_{NSE} amplitude following Eq. 3. The exact averaging will depend on the distribution of the neutron trajectories which is determined by the characteristic of the incoming neutron beam defined by the collimation or the neutron guide optics. Furthermore, this effect becomes most prominent with increasing the neutron beam wavelength.

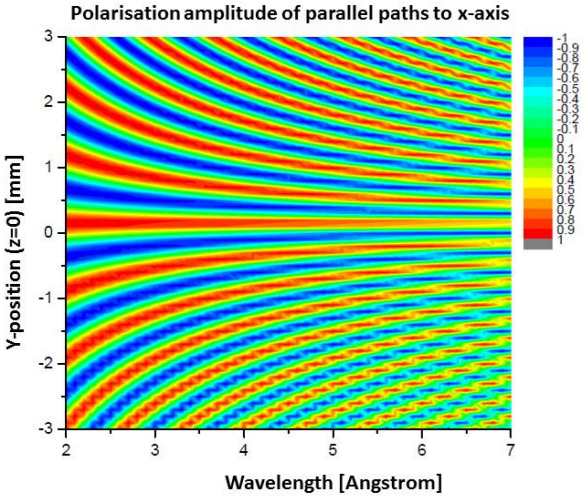

*Figure 10: Contour plot of the spin echo modulation P_{NSE} (Eq. 2 and 6), calculated for neutron trajectories parallel to the central one (*dotted line in Fig.1). The next step was to consider the effect of the beam divergence on the examples of the 7 individual neutron trajectories non-parallel to the x-axis shown in Fig.6.

The configuration used for the magnetic field calculations had an overall length of 3.1 m and reproduced a test setup used for an experiment at the HZB, on the V20 ESS test beamline (to be published). In the following we will consider the requirements that must be met when downscaling the setup to a compact instrument. Without additional magnetic field calculations it is relatively simple to down scale the dimensions of the field arrangement and introduce a scaling factor S. Scaling means that all the dimensions, [x,y,z], are multiplied with the scaling factor S, so if the instrument is scaled down to half it size all [x,y,z] dimensions are multiplied by S=0.5. Despite the reduction of all the component dimensions we assumed that:

- The absolute magnetic field value in de DC magnets remains the same as this is coupled to the performance of the RF flippers.
- The beam cross-section/size remains unchanged.

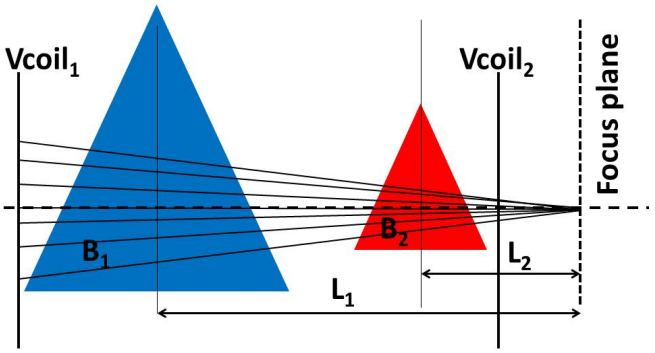

Figure 11: schematic top-view of the SEMSANS field arrangement with divergent neutron trajectories that all merge on the same position (y=0, z=0) of the focus plane

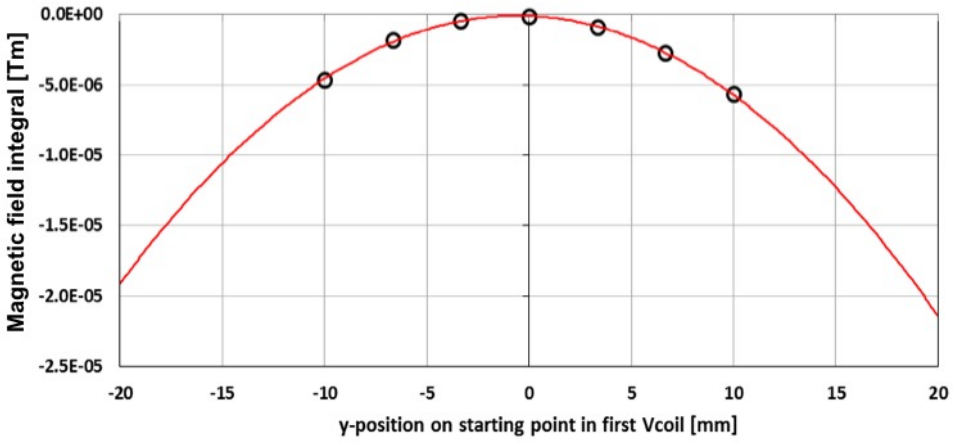

Figure 12: Magnetic field integral taken from the beginning to the end of the precession area (thus from the first to the last Vcoil) for all trajectories shown in Fig. 11. The solid line is an order polynomial fit to the data.

This means one can design the instrument in an arbitrary scale with the correct and optimized [x,z,y] ratios for the components, only leaving the scaling factor as a variable for the final size. However, the reduced dimensions should not affect the adiabaticity of the setup. Scaling down the arrangement of the DC magnets will increase ω_g and thus decrease the adiabaticity parameter k, proportional to the downscaling of the dimensions. Furthermore, if the beam cross-section does not change although the magnet is getting smaller the B_x component (Fig. 8) will increase, which will also linearly decrease the value of the adiabaticity parameter k. The combination of these two effects leads to the relation for the scaling factor S:

$$k_{scaled} = k_{original}\, S^2 \implies S = \sqrt{k_{scaled}/k_{original}} \tag{9}$$

This means that for the case investigated the scaling factor should consider only the adiabaticity. For the setup investigated with an overall length of 3.1 m the lowest k-value was 80 (Fig. 8). Assuming a minimum k-value of 10, leads to $S = \sqrt{80/10} = 2.8$. This will reduce the precession region length, i.e. the distance between the $Vcoil_1$ and $Vcoil_2$, from 3.1 m to 1.1 m, which can be considered as the minimal length for such a setup. Furthermore, as the pole shoes get smaller the effect of the beam divergence on the field integral will increase. Results, such as those provided in Fig. 12 can be used to evaluate the impact of this effect. If all parameters are scaled, including the magnetic field, obviously no additional magnetic field calculations are required.

References

[1] F. Mezei; Neutron Spin Echo, Lecture Notes in Physics, **128**, Springer, (1980), 3.
Mezei, F.; Pappas, C.; Gutberlet, T; Lecture Notes in Physics, **601**; Springer (2003).

[2] M.T. Rekveldt; *Nucl. Instrum. Methods Phys. Res. B*, ***114*** (1996) 366.

[3] M.T. Rekveldt; W. Kraan; T. Keller; *J. Appl. Crystallogr.*, ***35*** (2002) 28.

[4] O. Schärpf; F. Mezei (Ed Neutron Spin Echo, Lecture Notes in Physics, **128**, Springer, (1980), 28.

[5] F. Mezei; Neutron Spin Echo, Lecture Notes in Physics, 128, Springer, (1980) 178.

[6] C. Zeyen and P. Rem; Meas. Sci. Technol., **7** (1996) 782.

[7] S. Pasini and M. Monkenbusch; Meas. Sci. Technol., **26** (2015) 035501.

[8] O. Chubar, P. Elleaume, and J. Chavanne; J. Synchrotron. Rad., 51 (1998) 48.

[9] R. Gähler, A certain class of beam modulation techniques and its potential applications, PNCMI Polarised Neutron School, 2006.

[10] W.G. Bouwman, C.P. Duif, R. Gähler; *Physica B,* ***404*** (2009) 2585.

[11] W.G. Bouwman, C.P. Duif, J. Plomp, A. Wiedenmann, R. Gähler; *Physica B*, ***406*** (2011) 2357.

[12] A. Kusmin, W.G. Bouwman, A. A. van Well, C. Pappas; *Nucl. Instrum. Methods Phys. Res. A*, ***856*** (2017**)** 119.

[13] R. Gähler, R Golub; Neutron Resonance Spin-Echo, *Journal de Physique*;**49**, (1988) 1195.

[14] J. Plomp; Spin-echo development for a time-of-flight neutron reflectometer, Ph.D. Thesis, Delft, 2009.

[15] W. Kraan, M.T., Rekveldt, P. Por; *Nucl. Instrum. Methods Phys. Res.A*, **300** (1991) 35.
W. Kraan, et al.; *Nucl. Instrum. Methods Phys. Res.* A, **510** (2003), 334.